



**HAL**  
open science

## In situ observation of the capillary infiltration of molten silicon in a SiC/SiC composite by X-ray radiography

H. Carpentier, O. Caty, Y. Le Petitcorps, Eric Maire, A. Marchais, N. Eberling-Fux, G. Couegnat

### ► To cite this version:

H. Carpentier, O. Caty, Y. Le Petitcorps, Eric Maire, A. Marchais, et al.. In situ observation of the capillary infiltration of molten silicon in a SiC/SiC composite by X-ray radiography. Journal of the European Ceramic Society, 2022, 42, pp.1947-1954. 10.1016/j.jeurceramsoc.2021.12.041 . hal-03763025

**HAL Id: hal-03763025**

**<https://hal.science/hal-03763025>**

Submitted on 22 Jul 2024

**HAL** is a multi-disciplinary open access archive for the deposit and dissemination of scientific research documents, whether they are published or not. The documents may come from teaching and research institutions in France or abroad, or from public or private research centers.

L'archive ouverte pluridisciplinaire **HAL**, est destinée au dépôt et à la diffusion de documents scientifiques de niveau recherche, publiés ou non, émanant des établissements d'enseignement et de recherche français ou étrangers, des laboratoires publics ou privés.



Distributed under a Creative Commons Attribution - NonCommercial 4.0 International License

# In situ observation of the capillary infiltration of molten silicon in a SiC/SiC composite by X-ray radiography

H. Carpentier, O. Caty, Y. Le Petitcorps, E. Maire,  
A. Marchais, N. Eberling-Fux, G. Couégnat

December 9, 2021

## Abstract

Capillary infiltration is an innovative fabrication method for metal and ceramic-matrix composites. SiC/SiC composites can be infiltrated by molten silicon to decrease residual porosity. Physical and chemical mechanisms involved during Liquid Silicon Infiltration (LSI) are complex to analyze. An in situ observation setup for capillary infiltration of molten silicon has been designed for synchrotron observations. The setup reproduces the extreme high temperature and high vacuum conditions used in the LSI process. It is also designed for X-ray observations in synchrotron beamlines and tomography stages. Sets of 2D X-ray absorption radiographs were acquired at high frequency during the LSI process. The study outlines the capillary infiltration mechanisms of molten silicon inside SiC/SiC composites. It proves that full saturation of the composite is not directly achieved after the rise of molten silicon. It is a two step mechanism. First, the infiltration occurs inside the intra granular porosity of the SiC powder matrix. Then, larger scale porosities such as cracks are filled. These phenomena have been discussed previously in the literature but never observed in situ.

Key words : X-ray, radiography, in situ, capillary, infiltration, high vacuum, high temperature, Liquid Silicon Infiltration, Melt Infiltration, molten, silicon.

## 1 Introduction

SiC/SiC material composites are designed for applications in extreme conditions such as high temperature environment, oxidant or corrosive atmospheres. Their low density in combination with optimised mechanical and thermal properties make them a relevant choice for aerospace and nuclear applications (Krenkel, 1999; Christin, 2002; Naslain, 2004). These composites are obtained by mixing a SiC matrix with SiC fibres. They can be elaborated by means of ceramic process (suspension of SiC powder), gaseous process (Chemical Vapour Infiltration), or liquid process (Polymer Impregnation and Pyrolysis/ Reactive Melt Infiltration). Yet, in order to achieve dense composites, the above means of fabrication are often combined. For example, Liquid Silicon Infiltration (LSI), also called Melt Infiltration (MI), generally comes at the end of the process in order to reduce residual porosity (Gray, 2006). However, this step is not fully mastered and may result in non-infiltrated areas inside the composite. As it is difficult to observe the capillary rise of molten silicon at 1500 °C, some authors have developed devices to follow the height or the mass during the infiltration (Einset, 1998; Roger et al., 2018; Marchais, 2016; Sangsuwan et al., 1999; Kumar et al., 2009). It is assumed that the liquid silicon infiltration inside SiC/SiC composites follows a modified Washburn law with an effective diameter representative of the porous medium. The use of organic model fluids is generally adopted for a preliminary proper determination of the infiltration kinetic in the porous medium and to extract the effective diameter prior to silicon infiltration. For instance, the capillary rise of hexadecane is used to extract the effective diameter (Marchais et al., 2016). However, the effective diameter changes with temperature, in particular during the heat treatment necessary before LSI to remove non wetting barriers (Roger et al., 2018; Marchais, 2016). The pore sizes of the SiC matrix have a tendency to irreversibly increase at high temperature making the prediction of silicon rise questionable by extrapolating the sole hexadecane results (Roger et al., 2020a).

Alternatively, it is possible to better capture the silicon infiltration mechanisms by interrupting the process before saturation even if it is difficult to operate since the capillary rise speed is high (0.4 mm/sec) as long as the sample is hot. Marchais et al. managed to stop the process and made tomographic and microscopic observations (Marchais, 2016). They show that the silicon first rises inside the micro porosities of the powder avoiding the larger scale pores of the composite such as shrinkage cracks. Thus, the wetting front saturation is not total as it is in the case of a SiC compact powder. This was already sensed during hexadecane infiltrations of SiC compact powder and SiC/SiC composites where the author could observe, in the case of composites, a discrepancy between the mass calculated from the height followed by a camera and the mass recorded by a weighing device. This difference was explained by the visible front height that corresponds only to the progression of the liquid inside the inter grains porosities and not to the saturation of the whole medium underneath (yarns and powder matrix).

More recently, (Roger et al., 2020b) proved that single component materials exhibiting a multi scale porosity are infiltrated according to a two-step mechanism both at low temperature with hexadecane and at high temperature with silicon. The kinetic is divided into two parts both following a modified Washburn law. The first one is associated with the impregnation of small porosities and the second one corresponds to the infiltration of larger pores. Although these two stages are both observed at low and high temperature, the kinetics on the same samples are very different. For instance, molten silicon

can fill larger pores than hexadecane and at a greater speed. These differences could be explained by the much lower capillary number of hexadecane. The authors conclude that organic fluids are relevant to predict infiltration mechanisms at high temperature but are not sufficient to predict kinetics of molten silicon.

The aim of this work is to develop a new approach to observe the capillary rise of molten silicon inside a complex material such as a SiC/SiC composite. One objective is to confirm mechanisms proposed in the literature and to give further insights on high temperature phenomena that could occur, such as gas trapping or reactive infiltration.

The use of synchrotron X-ray beam for the in situ observation of a fabrication process has been proven to provide valuable information. For instance, the microstructure evolution has been imaged during axial impregnation of unidirectional ceramic fibre beds and pyrolysis of a SiC-based preceramic polymer to 1200 °C (Larson and Zok, 2018a,b; Larson et al., 2019). Our work follows the path of a large number of experimental setup developed for synchrotron X-ray in situ observation (Maire et al., 2016; García-Moreno et al., 2018, 2019; Mazars et al., 2017; Turpin et al., 2021; Youssef et al., 2013).

The paper will first present the device developed to in situ observe capillary rise using X-ray radiations at high frequency. Then, results obtained under synchrotron X-Ray radiation will be presented and discussed. Image treatments and analysis are developed to confirm or propose infiltration mechanisms in SiC fibre complex media. Capillary rise velocity are measured in different areas to identify morphological parameters and, to better understand the underlying physical and chemical mechanisms.

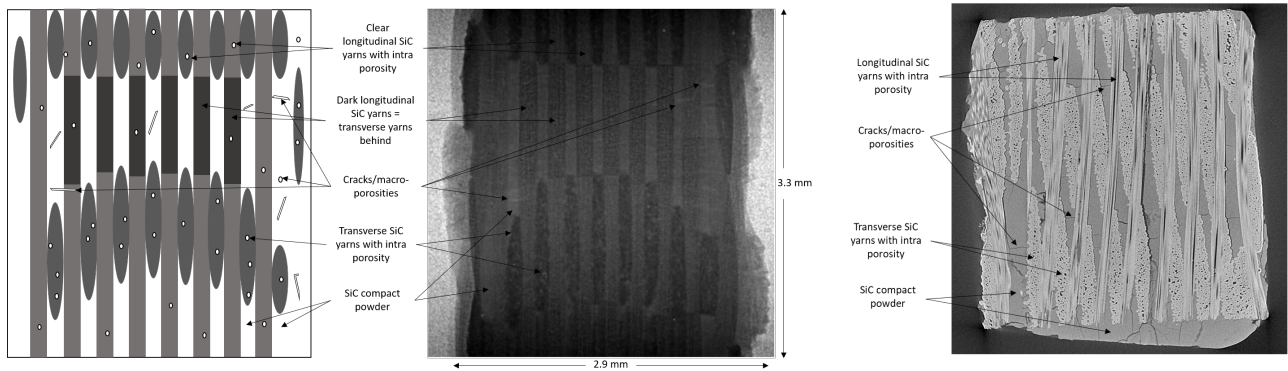
## 2 Materials and methods

### 2.1 Materials

For this study, the material was a SiC/SiC composite manufactured by Safran Ceramics. It is composed of BN coated-fibre preform where each yarn is made of approximately 500 fibres (Hi-Nicalon S). The preform is of type 2D interlock with longitudinal rectilinear yarns and transverse tortuous yarns woven through several layers. The latter is first consolidated with SiC by the mean of CVI (Chemical Vapour Infiltration). Later, an aqueous suspension of SiC powder is injected inside the preform and dried in order to process the SiC matrix of the SiC/SiC composite (Slurry Cast process) (Luthra and Corman, 2006). The drying process can lead to defects such as cracks. Finally, the material is thermally treated to remove non wetting barriers before final Melt Infiltration step.

For the in situ study, the dimension of the specimen was designed to visualise the whole section at a resolution of 2.75  $\mu\text{m}$ . Rectilinear specimens of height 100 mm and of cross section  $3 \times 3 \text{ mm}^2$  were machined from a plate with prior SiC CVI reinforcement and SiC slurry injection, following the industrial process. A further thermal treatment of 12 h at 1400 °C under high vacuum was performed before the impregnation. The liquid used was a silicon-boron alloy to prevent excessive reactive infiltration.

The initial state of the material is presented on Figure 1. Before infiltration the difference between yarns and compact powder is clearly visible. Some cracks are also present and radiograph are enough to isolate them but not to visualise their complete shape.



(a) Scheme and radiograph of sample 1 with different parts highlighted (lateral view).

(b)  $\mu$ CT cross section of the sample.

Fig. 1: SiC/SiC composite before infiltration.

## 2.2 Methods

### 2.2.1 Material characterization before synchrotron experiment

Pore size distribution and porosity was measured by mercury intrusion porosimetry (Autopore IV, Micromeritics Instrument Corp., USA) for a sample volume of  $0.7 \text{ cm}^3$ .

Capillary infiltration experiments were performed on a modified commercial tensiometer (Tensio-Cad W TE-5200 MO, CAD Instrument, France) operating at  $20 \text{ }^\circ\text{C}$  in a temperature regulated room. Hexadecane was used as a solvent for its low volatility (saturation vapor pressure :  $4.88 \times 10^{-2} \text{ Pa}$ ). This experiment is repeatable and non destructive.

The X-ray computed tomography (CT) on Figure 1b was obtained on a laboratory tomograph (GE v|tome|x s research edition, General Electrics, USA) using a  $140 \text{ kV}$  X-ray source with an intensity of  $60 \text{ } \mu\text{A}$ . A  $500 \text{ ms}$  exposure time and a spatial resolution of  $3 \text{ } \mu\text{m}$  per voxel unit were achieved. These measurements revealed the 3D architecture of the samples schematized on Figure 1a.

### 2.2.2 High temperature infiltration device for in situ observation

For the in situ silicon infiltration tests, a specific device has been developed. It had to support high vacuum to prevent any oxidation of the SiC/SiC sample or silicon. A small layer of  $\text{SiO}_2$  is sufficient to prevent the wetting and hence block the infiltration (Drevet and Eustathopoulos, 2012). Moreover, capillary infiltration is only possible at temperatures above the silicon melting point :  $1414 \text{ }^\circ\text{C}$ . The device is thus a heating vacuum chamber (Figure 2). that fits on a synchrotron tomograph base plate. It is then possible to measure and control vacuum and temperature. The chamber enables a vacuum of  $10^{-5} \text{ mbar}$  thanks to a turbo pump (HiCube 80 Pfeifer) and temperatures up to  $1600 \text{ }^\circ\text{C}$  by induction heating (Fives Celes generator). One pipe is dedicated to the X-ray visualization. The windows are made of Kapton tape to limit the absorption of X-ray and ensure the high vacuum. The height of these windows has been chosen to align the X-ray synchrotron source and the middle height of the

sample. A linear actuator enables a precise vertical positioning ( $\pm 0.1$  mm) of the sample with 50 mm of vertical displacement, which is sufficient to immerse the sample in the melt.

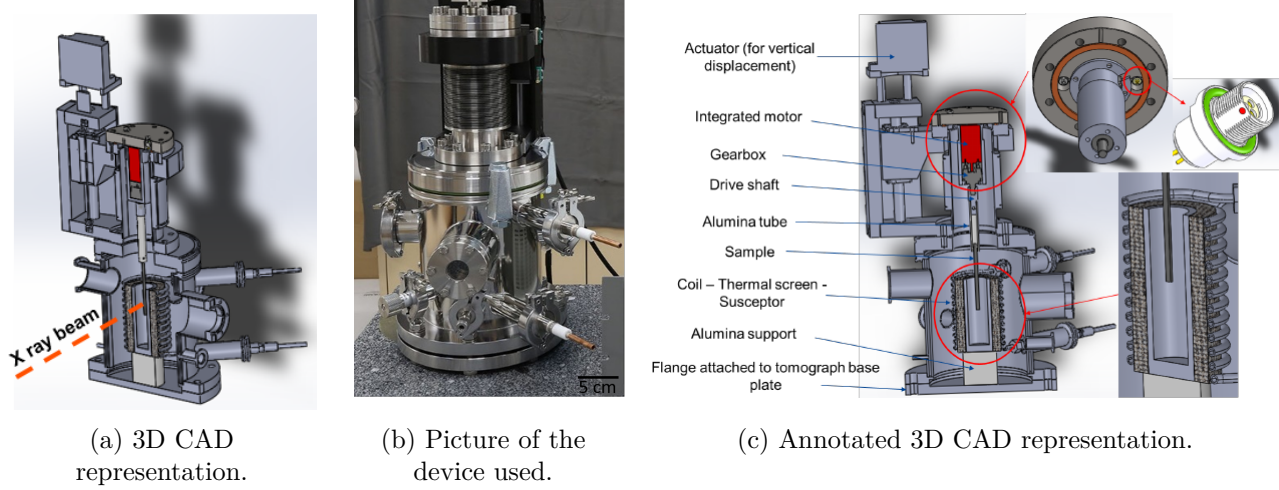


Fig. 2: General description of the heating vacuum chamber for capillary infiltration.

### 2.2.3 Experimental process

Once the chamber reaches  $10^{-5}$  mbar, everything is heated up to  $1400$  °C at  $10$  °C/min for 1 hour to homogenize the temperature and remove wetting barriers. Then, the infiltration occurs at  $1450$  °C after 30 minutes of heating to melt the silicon-boron alloy. During this cycle, the sample is kept at a safety distance of 2 cm from the melt to prevent early infiltration. Then, the sample is lowered at  $1$  mm/s until the liquid position is reached. Radiographs are recorded until complete infiltration of the sample.

### 2.2.4 X-ray acquisition

A GigaFRost camera was used with a 4x optical magnification microscope (Mokso et al., 2017). It allows a field of view (FOV) of  $3.3 \times 3.3$  mm<sup>2</sup>. As a first experimental campaign, only radiographs were recorded at a rate up to 50 Hz using a 40 keV X-ray source. Two sets of measurement are further analyzed and are referred as infiltration 1 and infiltration 2. The first one was recorded with a frame rate of 11.11 projections per second whereas the second one had a frame rate of 50 Hz. Both infiltrations took place under the same experimental conditions and the samples were manufactured following the same procedure, as described in section 2.1.

### 2.2.5 Data analysis

Raw radiographs were post treated in order to highlight the infiltration mechanisms. First, a flat field correction is made to remove noise. For this purpose, projection images without sample are acquired with and without the X-ray beam turned on, which are referred to as flat or white fields ( $W_i$ ) and

dark fields ( $D_i$ ).  $D$  and  $W$  are taken as the average of 100 acquisitions. The corrected image ( $C$ ) is obtained by applying the following operation to  $N$ , the original image :

$$C = \frac{N - D}{W - D}$$

In addition, the first image of the stack ( $n_0$ ) can be subtracted from the stack of projections ( $n_i$ ) to make the infiltration mechanisms more visible.

Finally, the Reslice function was used in *Fiji* software. It generates a “side-view” of the stack along a line drawn in the region of interest of the stack of radiographs. Here, the 3<sup>rd</sup> dimension ( $Z$ ) is not spatial but temporal since the slice number is proportional to time. The “side-view” gives the evolution of the gray values along this line against time. This function analyze the gray value change and enables to spot the very locally silicon alloy rise. It can be also used to extract kinetics information (e.g. local speed of infiltration) as further discussed in section 3.6.

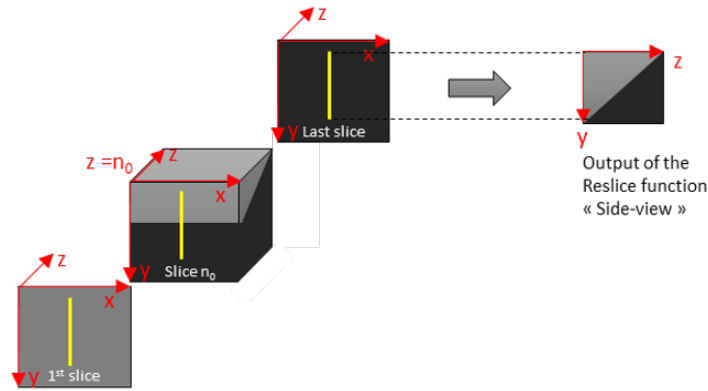


Fig. 3: Reslice of a line experiencing a change of gray value along the stack.

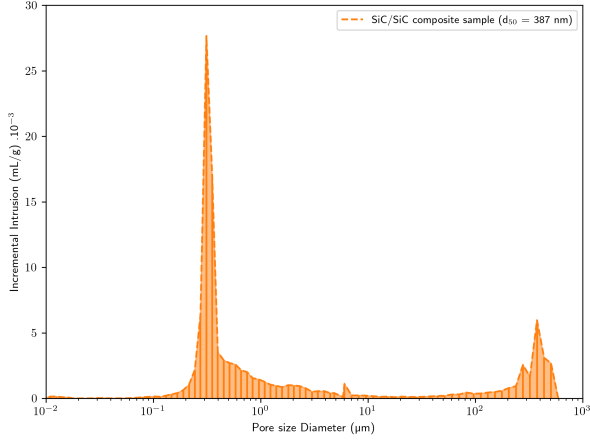
### 3 Results

#### 3.1 Pore size distribution and infiltration kinetics at room temperature

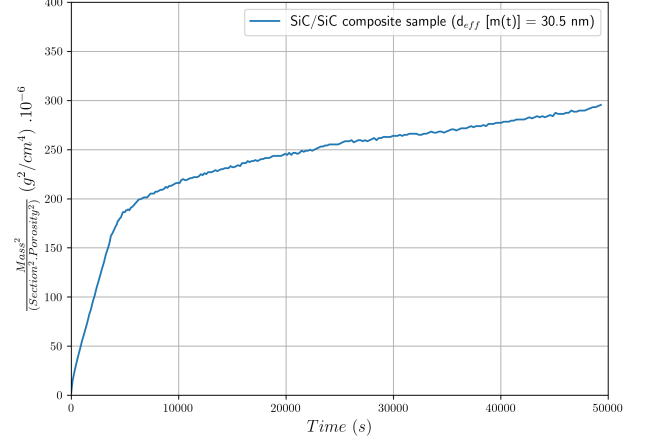
Before melt infiltration, the SiC/SiC composite exhibits a multi scale porosity as shown by the mercury intrusion experiment (Figure 4a). Macro porosity, located inside the yarns or in the drying cracks, is in the size of [50-600]  $\mu\text{m}$ . The micro porosity corresponds to the inter-grains porosity of the SiC powder matrix and corresponds to the 350 nm peak on Figure 4a. The median pore diameter is 387 nm.

A classical Washburn experiment was conducted at room temperature beforehand to estimate the capillary infiltration kinetics at high temperature. A two step infiltration mechanism is observed on Figure 4b, which is consistent with the multi scale porosity of the sample. The first regime of infiltration is attributed to the filling of inter-grain porosity whereas the second regime is explained by the presence of macropores that take more time to be completely infiltrated. During melt infiltration,

similar mechanisms are expected even though they should be faster as evidenced by (Roger et al., 2020a,b).



(a) Pore size distribution of a SiC/SiC composite sample.

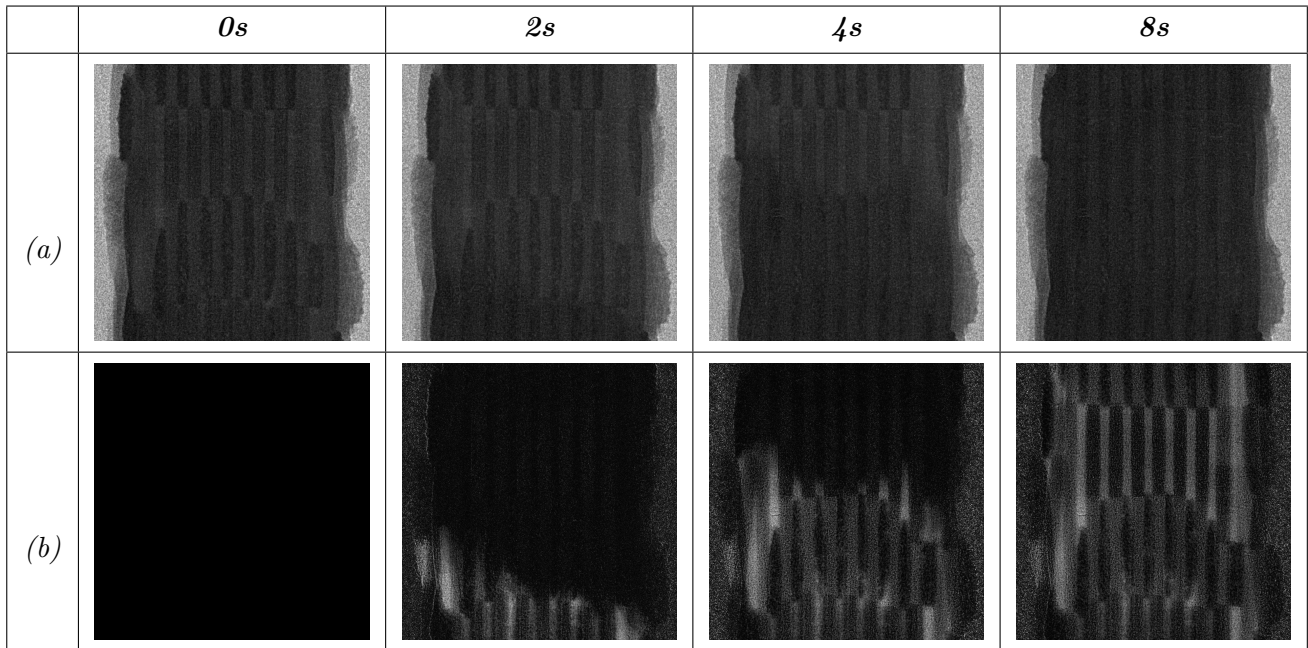


(b) Time dependence of the squared weight gain curves normalized to the section during hexadecane capillary rise.

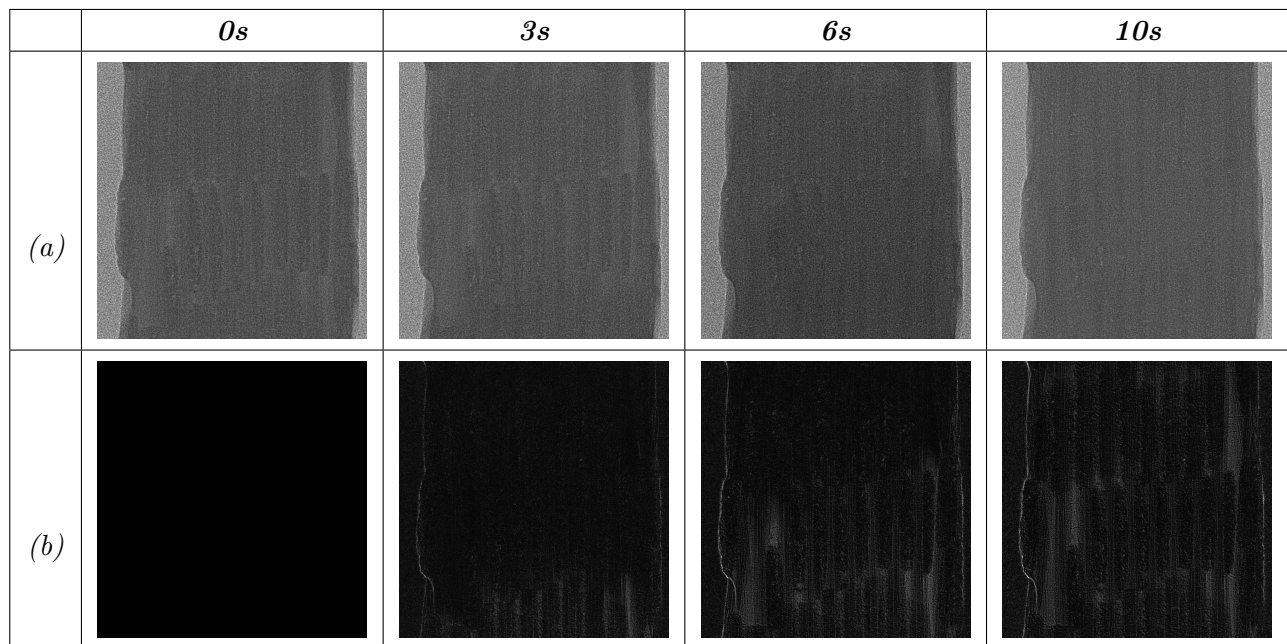
Fig. 4: SiC/SiC composite characterization before melt infiltration.

### 3.2 In situ observation of the silicon wetting front rise : 1<sup>st</sup> step in the filling mechanisms ( $t < 10s$ )

Raw images of the rising front during the first step of densification, at very early moments of infiltration ( $t < 10s$ ), are gathered in Tab. 1. (a) and Tab. 2. (a). The wetting front rises in  $\Delta t_1 = 8 s$  for infiltration 1 and  $\Delta t_1 = 10 s$  for infiltration 2. The subtraction of the first image  $n_0$  (1<sup>st</sup> image of the 1<sup>st</sup> filling mechanism) from the stack of projections is presented in Tab. 1. (b) and Tab. 2. (b).



Tab. 1: Rising front during infiltration 1 - (a) Raw images with flat field correction, (b) Difference between images and the initial state ( $n_i - n_0$ ) to highlight the front.



Tab. 2: Rising front during infiltration 2 - (a) Raw images with flat field correction, (b) Difference between images and the initial state ( $n_i - n_0$ ) to highlight the front.

One can immediately note that the silicon alloy infiltration front is not planar. It goes inside the SiC powder matrix (in light gray), inside longitudinal yarns (in darker gray, indicating a smaller amount of infiltrated silicon) and inside transverse yarns (mostly visible on infiltration 2). In terms of saturation, transverse yarns appear darker in the difference images, which indicates a lack of silicon into these areas during the infiltration. It has to be noted that the amount of BN coating was not sufficient to prevent the silicon from rising first at the surface of the sample during infiltration 2 as indicated by the light gray skin visible on Tab. 2. (b). Finally, one can notice that SiC powder matrix is not fully saturated with remaining unfilled cracks. These mechanisms are highlighted on Figure 5.

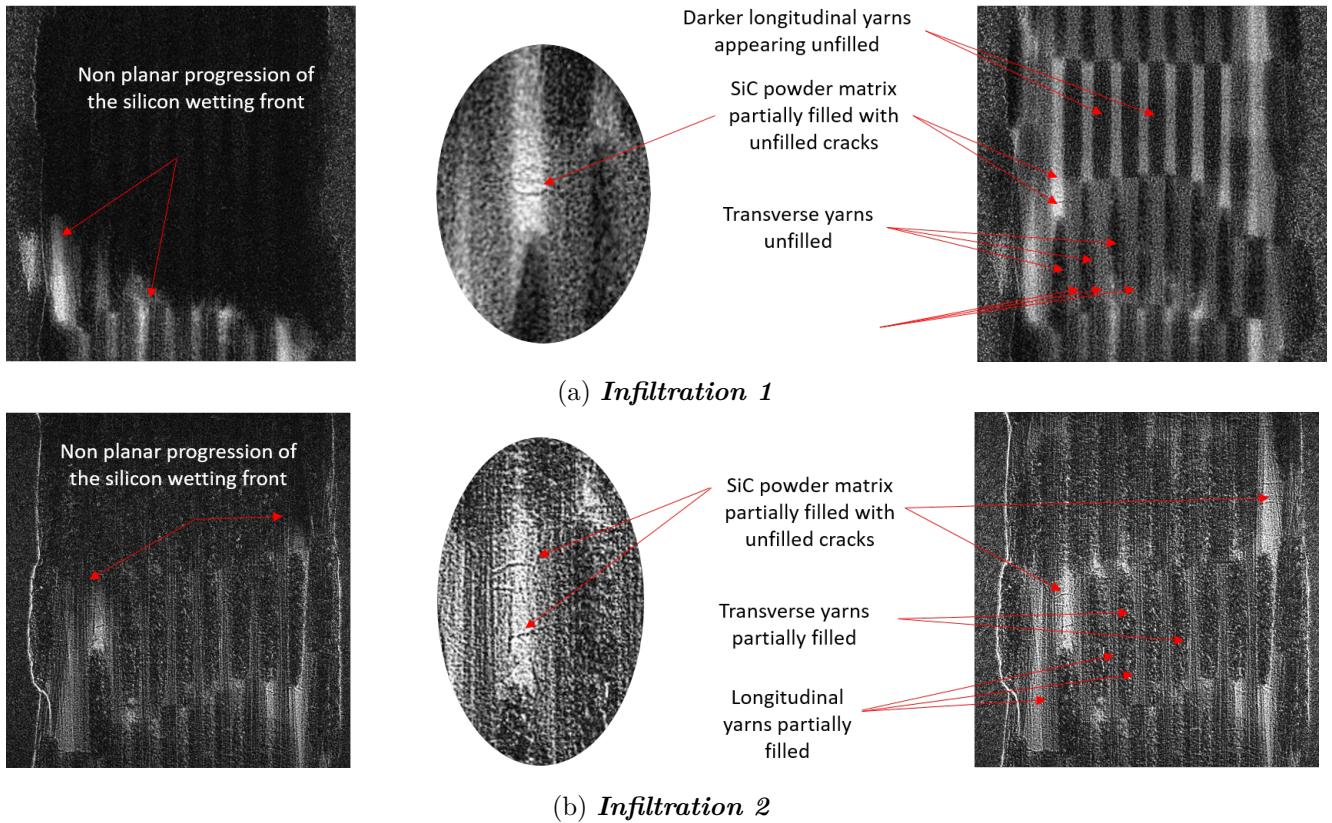
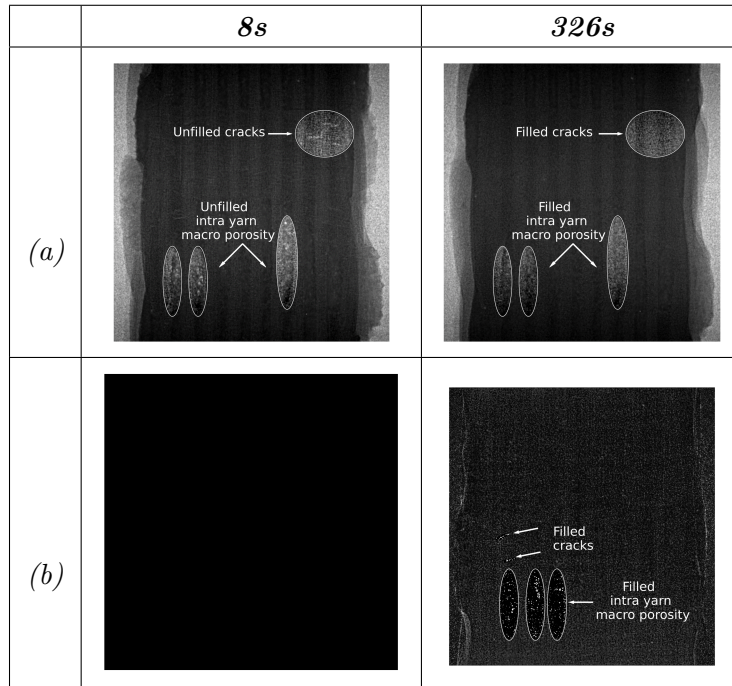


Fig. 5: Infiltration mechanisms for (a) sample 1 and (b) sample 2.

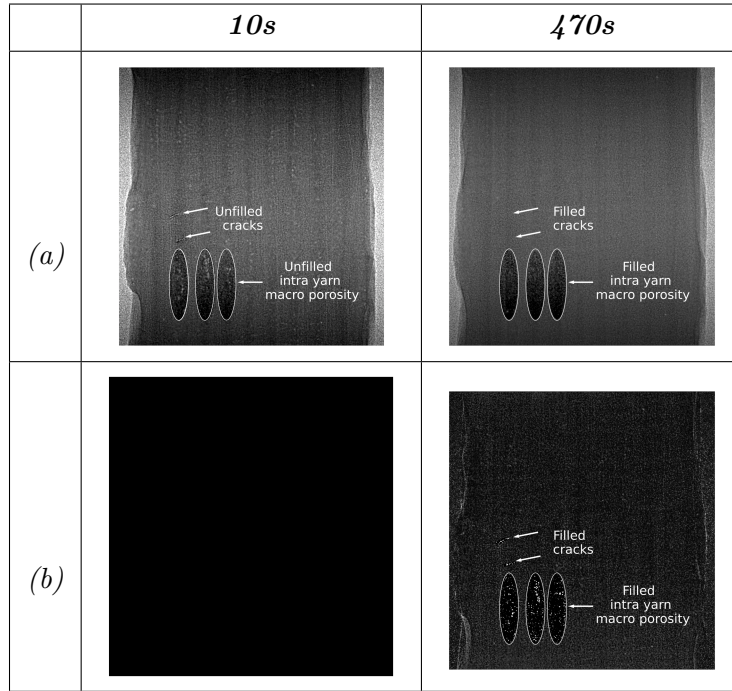
### 3.3 In situ observation of the macro porosities filling: 2<sup>nd</sup> step in the filling mechanisms

The second step occurs right after the initial silicon front rise ( $t > 10s$ ). Both samples get darker with the progressive filling of the macroporosity. Filled areas are difficult to spot on radiographs since it represents a small amount of liquid but most visible areas are circled in red on Tab. 3 and Tab. 4. Most of the porosities are filled at the end of this 2nd filling mechanism, including cracks inside the SiC powder matrix as well as the intra yarn macro porosity that is mainly visible within the transverse yarns.

The most visible filling lasts  $\Delta t_2 = 175$  s for infiltration 1 and  $\Delta t_2 = 142$  s for infiltration 2. In the end, during both infiltration 1 and 2, the liquid seems to expand along the borders of the sample during  $\Delta t_{2_{bis}} = 143$  s and  $\Delta t_{2_{bis}} = 318$  s respectively.



Tab. 3: Filling of macropores (state 1 to 2) during infiltration 1 - (a) Raw images, (b) Difference between the different states ( $n_1 - n_1$ ,  $n_2 - n_1$ ).



Tab. 4: Filling of macropores (state 1 to 2) during infiltration 2 - (a) Raw images, (b) Difference between the different states ( $n_1 - n_1, n_2 - n_1$ ).

### 3.4 Mean gray values and saturation analysis

Since only radiographs were analyzed, the filling is not always clearly visible. To better understand the infiltration mechanisms, a quantitative measure of the saturation process was calculated from the mean gray value of the images as :

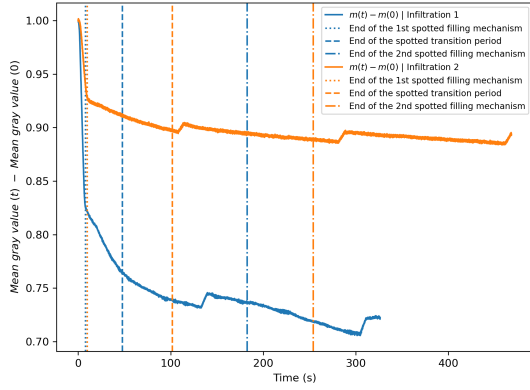
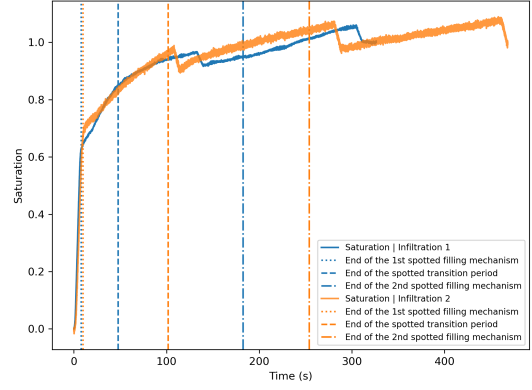
$$Saturation(t) = \frac{Mean\ gray\ value(t) - Mean\ gray\ value(t_0)}{Mean\ gray\ value(t_2) - Mean\ gray\ value(t_0)}$$

with the following assumptions :

$t_0$  : beginning of the observation = dry sample

$t_2$  : end of the observation = fully saturated sample

The results for infiltration 1 and 2 are given on Figure 6.

(a) Mean gray value (t) - Mean gray value ( $t_0$ ).

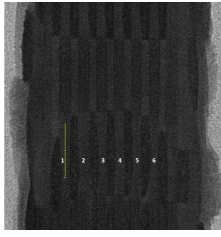
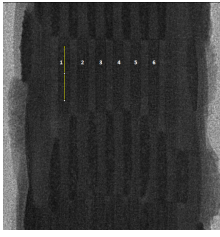
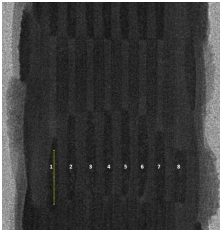
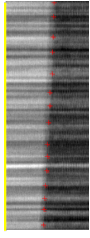
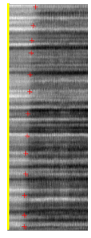
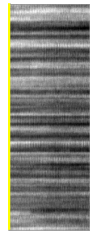
(b) Saturation (t).

Fig. 6: Mean gray values and saturation for infiltration 1 and 2.

This saturation analysis reveals the two fillings mechanisms that are well identified by a significant change of slope around  $t = 10$  s. Intermittent steps on the different curves are thought to be due to small movements of the samples during the infiltration.

### 3.5 Spatial study of the silicon rise

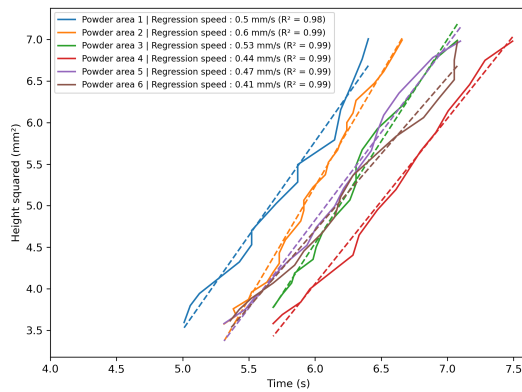
As explained in section 2.2.5, a reslice was performed to locally follow the silicon front along several lines located inside the matrix powder, longitudinal yarns and transverse yarns. Longitudinal yarns appear either in clear or dark shade of black, whether transverse yarns are located behind or not. Tab. 5. (a) indicates the position of the resliced areas and Tab. 5. (b) shows the result obtained for zone n°1 and are representative of the other zones identified in the whole sample (see also velocity results). The rise of silicon occurs inside the SiC powder matrix and clear longitudinal yarns with a high contrast before and after the silicon rise. In the transverse and dark longitudinal yarns, no clear change of contrast is observed during the silicon front rise. Images are absorption contrast radiographs, thus the resulting observation is the sum of kinetics through the whole sample. Hence, the following results give an overview of the spatial repartition of melt silicon inside the material but a 3D visualization would be necessary to observe the filling of the powder, the longitudinal and transverse yarns alone.

	<i>Powder</i>	<i>Clear longitudinal yarn</i>	<i>Dark longitudinal yarn</i>	<i>Transverse yarns</i>
(a)				
(b)				

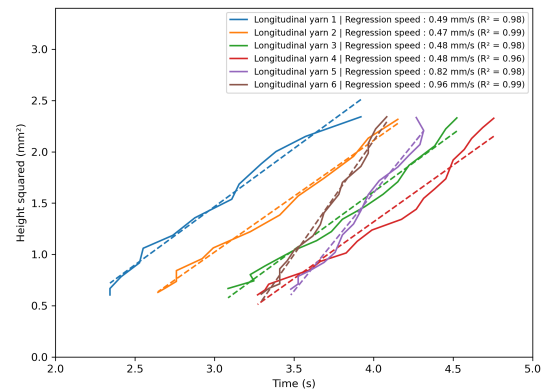
Tab. 5: Reslice of different areas in the sample 1 during front rise - (a) Position of the reslice treatment indicated by a yellow line, (b) Reslice output with light gray corresponding to non infiltrated areas and dark gray to infiltrated parts with melt silicon alloy.

### 3.6 Temporal study of the silicon rise

This reslice representation gives the evolution of the gray values along the different yellow lines. The velocity can then be extracted from the slope visible on the resliced images. Results are presented for the seven main SiC powder zones and six clear longitudinal yarns (Figure 7).



(a) Height squared as function of time and kinetics information in the different SiC powder areas.



(b) Height squared as function of time and kinetics information in the different longitudinal yarns.

Fig. 7: Kinetics information extracted from the reslice analysis of areas where the silicon rise is visible.

As anticipated, the evolution of the squared height as a function of time is linear for any SiC powder zone. The speed varies from 0.41 to 0.60 mm/s which is consistent with the fact that silicon front is not planar. The squared height is also effectively linear with respect to time for any clear longitudinal yarns. In these zones, the estimated speed varies from 0.47 mm/s to 0.96 mm/s. This maximum value shows that the rising speed of silicon can be twice higher in some areas. These values are slightly greater than the apparent speed reported in Tab. 6 ( $\frac{\Delta H}{\Delta t_1}$ ) which is normal since  $\Delta t_1$  corresponds to the time for all the silicon to reach the top of the observed zone ( $\Delta H$ ). The apparent speed ( $\frac{\Delta H}{\Delta t_1}$ ) is the smallest value of the local velocities (0.41 mm/s) which is in good agreement with the speed of infiltration reported in the literature (Marchais, 2016).

The linearity of  $height^2 = f(t)$  is an expected result since the silicon rise inside a composite would follow the modified Washburn law when monitoring the squared mass as function of time,  $mass^2 = f(t)$  (Roger et al., 2018, 2020b). Figure 7 presents the first mechanism of filling which would correspond to the first linear part of Figure 4b. If one were to follow simultaneously the height and the mass with respect to time during this experiment, a discrepancy should be observed when correlating the two dimensions since the wetting front is not completely saturating. The saturation takes place in a second step, matching the second linear part of Figure 4b. This had been previously reported in the literature when working at room temperature with similar composites (Marchais et al., 2016).

## 4 Discussion

### Global scenario of infiltration

Based on these data, it is possible to extract the filling mechanisms of the Liquid Silicon Infiltration (LSI) process. In a first step ( $\Delta t_1 < 10$  s), molten silicon rises under the shape of a non-planar front inside the micro porosities of the SiC powder first, avoiding cracks, macro pores and most of the intra yarn porosities (State 1, Figure 8). Yet, the experimental results have shown that some longitudinal and transverse intra yarns porosities are also filled during this phase. This could also be the result of powder located between transverse and longitudinal yarns. Conclusions are only drawn on 2D projections.

Then, a second and slower mechanism takes place with the filling of the macro porosity ( $\Delta t_2$ ). In the end, liquid seems to be expanding from the sample during  $\Delta t_{2_{bis}}$ .

This sequence is the same for each experiment but the intervals of time  $\Delta t_2$  and  $\Delta t_{2_{bis}}$  vary from one specimen to another as indicated in Tab. 6.

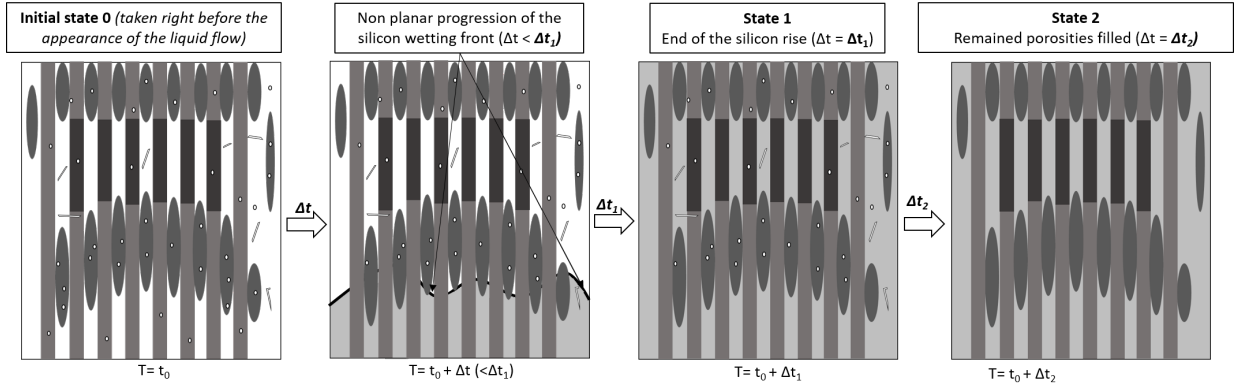


Fig. 8: Filling mechanisms of a SiC/SiC composite during molten silicon capillary infiltration.

Filling information	Infiltration 1	Infiltration 2
Rising front : 1 <sup>st</sup> filling $\Delta t_1$ (s)	8	10
Densification : 2 <sup>nd</sup> filling $\Delta t_2$ (s)	175	142
Liquid evolution at the border : $\Delta t_{2bis}$ (s)	143	318
Complete mechanism $\sum \Delta t$ (s)	326	470
Height of the observed area $\Delta H$ (mm)	3.3	3.3
Apparent (average) speed $V = \frac{\Delta H}{\Delta t_1}$ (mm/s)	0.41	0.36

Tab. 6: Summary of the filling information for infiltration 1 and 2.

The first filling is similar for infiltration 1 and 2 with similar rising times (8 s vs 10 s) and apparent (average) speed (0.41 mm/s vs 0.36 mm/s). Differences can be observed for the second filling that can be explained by the fact that macro porosity, such as cracks and intra yarn porosities, are not exactly the same from one sample to another. This amount can vary as it depends on the fabrication process. Consequently, the two samples have their own multi scale porosity architecture. In addition, the samples are very small and constitute just about a RVE (Representative Elementary Volume).

## 5 Conclusion

The device designed for this work proves the feasibility of using synchrotron X-ray for the in situ observation of the Melt Infiltration (MI) process occurring at 1500 °C under high vacuum. X-ray radiographs has been acquired with a 2.75  $\mu\text{m}$  resolution, at a rate up to 50 Hz which was sufficient to capture the transient fillings of CMC specimens.

The experimental results exhibit a two step filling mechanism of the SiC/SiC composites. At the very beginning, the molten alloy rapidly rises mainly inside the SiC intra granular porosity. The wetting front is not uniform. Then, a second filling has been observed that is slower and that corresponds to the filling of the bigger porosities such as cracks and intra yarn macro porosities.

These mechanisms have been highlighted and their speed has been quantified locally. The saturation

analysis confirmed the two filling mechanisms and revealed a significant change of infiltration rate. This work clearly shows that full saturation is not achieved directly after the rise of the wetting front during the Liquid Silicon Infiltration (LSI). However, it would benefit from additional 3D information to precisely quantify the localisation of the melt inside the complex and multi scale porosity of the composite.

The developed setup opens the perspective of a complete 3D tomographic in situ observation of the high temperature capillary infiltration to answer the remaining interrogations. An image based capillary infiltration model could then be developed from the 3D in situ data.

## **6 Acknowledgments**

The authors wish to acknowledge the Paul Scherrer Institut, Villigen, Switzerland for provision of synchrotron radiation beamtime at beamline TOMCAT of the Swiss Light Source. Christian Schlepütz and Gordan Mikuljan are warmly thanked for their kind assistance.

## References

- Christin, F. (2002). Design, Fabrication, and Application of Thermostructural Composites (TSC) like C/C, C/SiC, and SiC/SiC Composites. *Advanced Engineering Materials*, 4(12):903–912.
- Drevet, B. and Eustathopoulos, N. (2012). Wetting of ceramics by molten silicon and silicon alloys: A review. *Journal of Materials Science*, 47(24):8247–8260.
- Einset, E. O. (1998). Analysis of reactive melt infiltration in the processing of ceramics and ceramic composites. *Chemical Engineering Science*, 53(5):1027–1039.
- García-Moreno, F., Kamm, P. H., Neu, T. R., and Banhart, J. (2018). Time-resolved *in situ* tomography for the analysis of evolving metal-foam granulates. *Journal of Synchrotron Radiation*, 25(5):1505–1508.
- García-Moreno, F., Kamm, P. H., Neu, T. R., Bülk, F., Mokso, R., Schlepütz, C. M., Stampanoni, M., and Banhart, J. (2019). Using X-ray tomography to explore the dynamics of foaming metal. *Nature Communications*, 10(1):3762.
- Gray, P. E. (2006). Melt Infiltration of Ceramic Matrix Composites. page 5.
- Krenkel, W. (1999). Design of High Performance CMC Brake Discs. *Key Engineering Materials - KEY ENG MAT*, 164-165:421–424.
- Kumar, S., Kumar, A., Devi, R., Shukla, A., and Gupta, A. (2009). Kumar et al. - 2009 - Capillary infiltration studies of liquids into 3D Part B: Kinetics of silicon infiltration. *Journal of the European Ceramic Society*, 29(12):2651–2657.
- Larson, N. M., Cuellar, C., and Zok, F. W. (2019). X-ray computed tomography of microstructure evolution during matrix impregnation and curing in unidirectional fiber beds. *Composites Part A: Applied Science and Manufacturing*, 117:243–259.
- Larson, N. M. and Zok, F. W. (2018a). In-situ 3D visualization of composite microstructure during polymer-to-ceramic conversion. *Acta Materialia*, 144:579–589.
- Larson, N. M. and Zok, F. W. (2018b). Insights from in-situ X-ray computed tomography during axial impregnation of unidirectional fiber beds. *Composites Part A: Applied Science and Manufacturing*, 107:124–134.
- Luthra, K. L. and Corman, G. S. (2006). Melt infiltrated (MI) SiC/SiC composites for gas turbine applications. In *High Temperature Ceramic Matrix Composites*, pages 744–753. John Wiley & Sons, Ltd.
- Maire, E., Le Boulrot, C., Adrien, J., Mortensen, A., and Mokso, R. (2016). 20 Hz X-ray tomography during an in situ tensile test. *International Journal of Fracture*, 200(1-2):3–12.
- Marchais, A. (2016). *Etude des mécanismes de montée capillaire du silicium liquide au sein d'une préforme en carbure de silicium*. PhD thesis, Université de Bordeaux.

- Marchais, A., Roger, J., and Le Petitcorps, Y. (2016). Capillary infiltration of hexadecane in packed SiC powder and in SiC/SiC preforms: Pore description and calculation of molten Si infiltration. *Ceramics International*, 42(6):7774–7780.
- Mazars, V., Caty, O., Couégnat, G., Bouterf, A., Roux, S., Denneulin, S., Pailhès, J., and Vignoles, G. L. (2017). Damage investigation and modeling of 3D woven ceramic matrix composites from X-ray tomography in-situ tensile tests. *Acta Materialia*, 140:130–139.
- Mokso, R., Schlepütz, C. M., Theidel, G., Billich, H., Schmid, E., Celcer, T., Mikuljan, G., Sala, L., Marone, F., Schlumpf, N., and Stampanoni, M. (2017). GigaFRoST: The gigabit fast readout system for tomography. *Journal of Synchrotron Radiation*, 24(6):1250–1259.
- Naslain, R. (2004). Design, preparation and properties of non-oxide CMCs for application in engines and nuclear reactors: An overview. *Composites Science and Technology*, 64(2):155–170.
- Roger, J., Avenel, M., and Lapuyade, L. (2020a). Characterization of SiC ceramics with complex porosity by capillary infiltration: Part A - Filling by hexadecane at 20 °C. *Journal of the European Ceramic Society*, 40(5):1859–1868.
- Roger, J., Avenel, M., and Lapuyade, L. (2020b). Characterization of SiC ceramics with complex porosity by capillary infiltration: Part B – Filling by molten silicon at 1500 °C. *Journal of the European Ceramic Society*, 40(5):1869–1876.
- Roger, J., Guesnet, L., Marchais, A., and Le Petitcorps, Y. (2018). SiC/Si composites elaboration by capillary infiltration of molten silicon. *Journal of Alloys and Compounds*, 747:484–494.
- Sangsuwan, P., Tewari, S. N., Gatica, J. E., Singh, M., and Dickerson, R. (1999). Reactive infiltration of silicon melt through microporous amorphous carbon preforms. *Metallurgical and Materials Transactions B*, 30(5):933–944.
- Turpin, L., Roux, S., Caty, O., and Denneulin, S. (2021). Coupling tomographic and thermographic measurements for in-situ thermo-mechanical tests. *Measurement Science and Technology*, 32(3):035401.
- Youssef, S., Deschamps, H., Dautriat, J., Rosenberg, E., Oughanem, R., Maire, E., and Mokso, R. (2013). 4D imaging of fluid flow dynamics in natural porous media with ultra-fast x-ray microtomography. page 12.